The Structure and Evolution of Gap Outflow over the Gulf of Tehuantepec, Mexico

W. JAMES STEENBURGH

NOAA Cooperative Institute for Regional Prediction and Department of Meteorology, University of Utah, Salt Lake City, Utah

DAVID M. SCHULTZ

NOAA/National Severe Storms Laboratory, Norman, Oklahoma

BRIAN A. COLLE

Department of Atmospheric Sciences, University of Washington, Seattle, Washington

(Manuscript received 21 August 1997, in final form 10 December 1997)

ABSTRACT

Mesoscale-model simulations are used to examine the structure and dynamics of a gap-outflow event over the Gulf of Tehuantepec, Mexico, that was associated with a surge of cold air along the eastern slopes of the Sierra Madre. The simulated gap-outflow winds emerged from Chivela Pass, reached a maximum speed of 25 m s^{-1}, and turned anticyclonically as they fanned out over the gulf. Northerly winds were also able to ascend the mountains east, and to a lesser extent west, of Chivela Pass, indicating that the movement of cold air across the Sierra Madre was not confined to the pass. A mesoscale pressure ridge was aligned along the axis of the gap-outflow jet, which was flanked to the west by an anticyclonic eddy, and to the east by a weaker cyclonic eddy.

A model-derived trajectory along the axis of the outflow jet traced an inertial path, with anticyclonic curvature produced primarily by the Coriolis acceleration. The cross-flow pressure-gradient acceleration along this trajectory was negligible because it followed the axis of the mesoscale pressure ridge. Trajectories west (east) of the jet axis experienced stronger (weaker) anticyclonic curvature than expected from inertial balance because the cross-flow pressure-gradient acceleration produced by the mesoscale pressure ridge reinforced (opposed) the anticyclonic deflection by the Coriolis acceleration. As a result of these directional variations in the cross-flow pressure-gradient acceleration, a fanlike wind pattern was observed rather than a narrow jet.

Because of the large changes in SST and surface roughness that are observed during these gap-outflow events, better representation of these effects might improve future mesoscale-model simulations. Such improvements could be accomplished through coupled atmosphere–ocean mesoscale modeling, which could also be used to advance understanding of the oceanography of the gulf.

1. Introduction

Strong northerly surface winds that emerge from low-elevation gaps in the Sierra Madre and extend over the Gulfs of Tehuantepec, Fonseca, Papagayo, and Panama have a dramatic effect on the meteorology and oceanography of Mexico, Central America, and the eastern Pacific Ocean. Such winds occur most frequently in winter, when the cross-mountain pressure gradient is enhanced by a Central American cold surge, an equatorward-moving anticyclone along the eastern slopes of the Sierra Madre (Reding 1992; Schultz et al. 1997, 1998). Typical cold surges last 2–6 days (Schultz et al. 1998), producing northerly winds over the aforementioned gulfs that reach 10–20 m s^{-1}, with gusts of 60 m s^{-1} in extreme events (Stumpf 1975a,b; Trasviña et al. 1995). Over the Gulf of Tehuantepec, the leading edge of the strong northerlies is often marked by a line of convective clouds that is followed by blowing dust and heavy seas (Hurd 1929; Parmenter 1970; Stumpf 1975a; Schultz et al. 1997). The oceanographic response to the wind forcing includes the upwelling and entrainment of subsurface water into the surface layer, which can lower sea surface temperature (SST) by as much as 8°C in a few hours (Stumpf 1975b; Stumpf and Legeckis 1977; Legeckis 1988; Trasviña et al. 1995; Schultz et al. 1997). Nutrient-rich water is also brought to the surface, resulting in locally high phytoplankton concentrations that play an important role in the region's productive fishing industry (Fiedler 1994; García and Lluch-Cota 1996a, b; Lluch-Cota et al. 1997).

Corresponding author address: Dr. W. James Steenburgh, Department of Meteorology, University of Utah, 135 S. 1460 E., Room 819, Salt Lake City, UT 84112-0110.
E-mail: jimsteen@atmos.met.utah.edu

© 1998 American Meteorological Society

Favorable conditions for these wind events are created by the interaction of a Central American cold surge with the regional topography. The Sierra Madre, with crest heights of 2000–3000 m, extend southward and eastward through Mexico and Central America and represent the most prominent topographic feature of the region (Fig. 1a). This mountain range separates the Gulf of Mexico, Bay of Campeché, and Caribbean Sea from the Pacific Ocean. Although the Sierra Madre represent a significant barrier to low-level air masses, several mountain gaps allow for the channeling of air across Mexico and Central America. The most prominent is Chivela Pass (Fig. 1b), a 220-km long, 40-km wide gap from which northerly winds over the Gulf of Tehuantepec emerge. The terrain in this gap has a maximum elevation of only 250 m with peaks to its west reaching 2000 m, whereas those to the east approach 1500 m. Other important low-elevation gaps are located in Honduras near the Gulf of Fonseca, at Lake Nicaragua northeast of the Gulf of Papagayo, and on the Isthmus of Panama north of the Gulf of Panama (Fig. 1a). During a Central American cold surge, when high pressure is resident east and north of the Sierra Madre, *gap winds* [i.e., winds that are accelerated by an along-gap pressure gradient (Overland and Walter 1981)] are produced in these mountain gaps. The strong winds then extend downstream over the aforementioned gulfs. Over the Gulf of Tehuantepec, such *gap outflow* (i.e., an extension of a gap wind downstream of the terrain restriction) is known as a tehuantepecer (Hurd 1929; Huschke 1959) or tehuano (Trasviña et al. 1995).

Similar gap winds occur elsewhere including the Shelikof Strait of Alaska (Lackmann and Overland 1989), the Strait of Juan de Fuca between Washington and Vancouver Island (Reed 1931; Overland and Walter 1981), the Columbia River Gorge of Washington and Oregon (Cameron 1931; Cameron and Carpenter 1936; Decker 1979; Wolyn 1994), the Fraser River Valley of Washington and British Columbia (Mass et al. 1995), the Howe Sound of British Columbia (Jackson and Steyn 1994a,b), the Strait of Gibraltar between Spain and Morocco (Scorer 1952; Dorman et al. 1995), Vestfjorden, Norway (Jones et al. 1997), and the Cook Strait of New Zealand (Reid 1996). For long gaps, the cross-gap Rossby number, Vl/fL, where V is the along-gap wind speed, f is the Coriolis parameter, and l and L are the cross- and along-gap length scales, respectively, is usually $\ll 1$ (Overland 1984). As a result, approximate geostrophic balance develops in the cross-gap direction, with the Coriolis acceleration associated with the along-gap wind balanced by the cross-gap pressure-gradient acceleration (Overland 1984; Clarke 1988; Lackmann and Overland 1989). In the along-gap direction, scale analysis predicts a balance between pressure gradient and inertial accelerations (Overland and Walter 1981; Overland 1984). Observations reveal, however, that friction and entrainment ultimately limit the along-gap wind speed (Lackmann and Overland 1989).

While the studies listed above describe the flow within mountain gaps, relatively few studies have examined how gap winds evolve upon exiting a gap. Overland and Walter (1981) showed that a gap wind emerging from the Strait of Juan de Fuca transitioned rapidly from high speed (8–10 m s^{-1}) easterly flow to weaker (2–5 m s^{-1}) southeasterly flow. This transition occurred within 100 km of the exit of the strait and may have been associated with a hydraulic jump. Mass et al. (1995) described winds to the lee of the Fraser River Valley that accelerated rapidly as they moved over water, apparently due to changes in surface friction. The flow appeared to fan out and decelerate as it moved farther downstream.

In contrast, gap outflow over the Gulf of Tehuantepec can extend several hundreds of kilometers southward and westward over the eastern Pacific (Parmenter 1970; Stumpf 1975b; Legeckis 1988; Schultz et al. 1997) and appears to turn anticyclonically (Clarke 1988; Schultz et al. 1997). Clarke (1988) hypothesized that this anticyclonic outflow is inertially balanced. Under such conditions, the cross-flow pressure gradient is negligible and anticyclonic flow curvature is produced by the Coriolis acceleration. When viewed in the natural coordinate system (e.g., Holton 1992, 61–69), a balance exists between the Coriolis and centrifugal accelerations and parcels follow an inertial path with a radius of curvature R given by

$$R = -\frac{V}{f}, \tag{1}$$

where V is the wind speed and f is the Coriolis parameter. For $R < 0$, parcels turn toward the right (anticyclonically in the Northern Hemisphere). Evidence for such an inertial path has, however, been based primarily on indirect observations and theoretical studies. For example, Clarke (1988) argued that a region of relatively cold water produced in the Gulf of Tehuantepec during an outflow event was shaped in an arc that was consistent with an inertial path, and Schultz et al. (1997) suggested that cloud-band isochrones marking the leading edge of gap outflow followed an inertial path. The location or motion of these features, however, may not necessarily correlate with the path traced by air-parcel trajectories. In fact, studies examining limited wind observations have argued against an inertial path. Barton et al. (1993) and Trasviña et al. (1995) found that observed winds over the Gulf of Tehuantepec exhibited radii of curvature that were considerably smaller than that predicted by inertial balance. Barton et al. (1993) also illustrated that the gap outflow spreads out over the gulf rather than remaining confined in a narrow jet as suggested by the scale analysis presented by Clarke (1988).

This paper examines the structure and evolution of gap outflow over the Gulf of Tehuantepec during the Central American cold surge of 12–14 March 1993

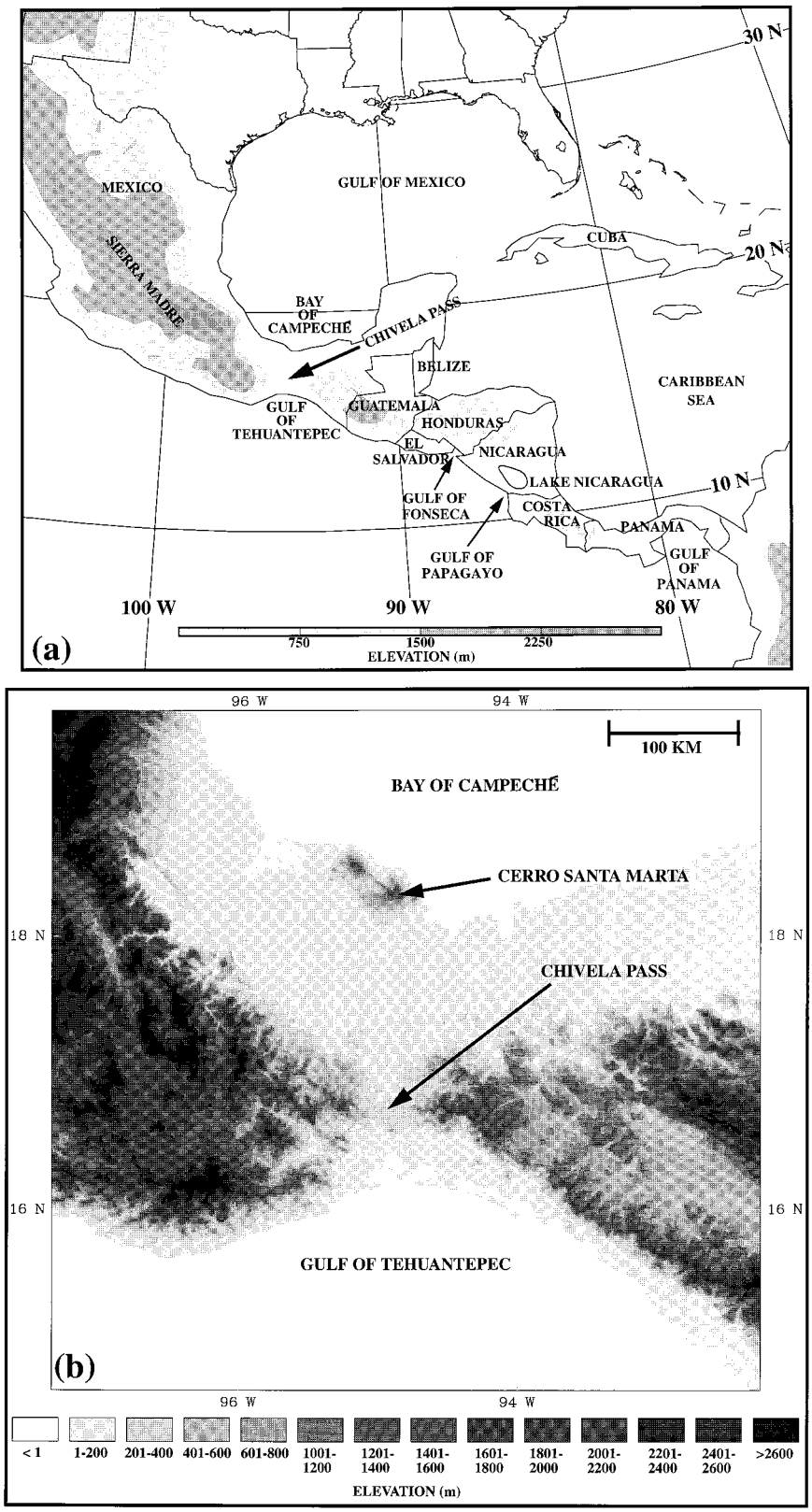

FIG. 1. Major terrain and geographic features of (a) Mexico and Central America (60-km MM5 terrain shaded according to legend) and (b) Chivela Pass region (30-s averaged terrain shaded according to legend).

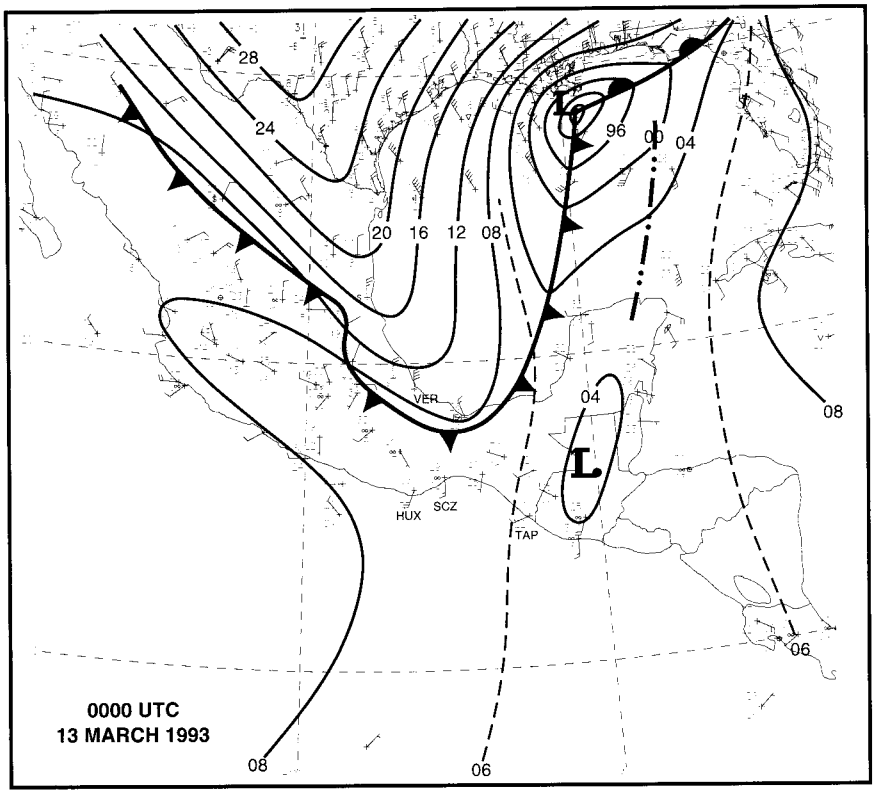

FIG. 2. Manually analyzed surface map for 0000 UTC 13 March. Sea level pressure every 4 hPa (solid) and every 2 hPa where needed to enhance analysis (dashed). Winds: one pennant, full barb, half-barb, and circle denote 25, 5, 2.5, and less than 1.25 m s^{-1}, respectively. Conventional frontal analysis and surface station reports. Dash–dot line represents a surface trough. Three-letter station identifiers discussed in text are included below station model.

(Schultz et al. 1997) using output from a high-resolution simulation by the Pennsylvania State University–National Center for Atmospheric Research Mesoscale Model version 5 (hereafter MM5). Section 2 summarizes the observational evolution of the event and is followed in section 3 by a description of the mesoscale model. The mesoscale structure and evolution of the simulated wind field over the Gulf of Tehuantepec is described in section 4. Section 5 compares the momentum balance in this region to that of inertial flow. A brief summary and motivation for future coupled atmosphere–ocean modeling of this phenomenon are presented in section 6.

2. Observational overview

From 12–14 March 1993, a rapidly deepening midlatitude cyclone known as Superstorm 1993 developed over the Gulf of Mexico and the eastern United States producing low pressure records, heavy snowfall, severe weather, and coastal flooding (Kocin et al. 1995; Uccellini et al. 1995; Caplan 1995; Huo et al. 1995; Bosart et al. 1996; Dickinson et al. 1997). In the wake of this system, a strong surge of cold air moved equatorward along the Sierra Madre into Mexico and Central America bringing 20 m s^{-1} winds and 15°C temperature falls (Schultz et al. 1997). Accompanying this cold surge were 20 m s^{-1} northerly gap-outflow winds over the Gulf of Tehuantepec that were marked at their leading edge by an arc-shaped rope cloud that appeared to trace an inertial path as it moved over the Pacific. The analysis presented in this section summarizes the atmospheric conditions preceding and during this gap-outflow event and is based on standard operational surface and upper-air datasets that were supplemented by Mexican and Central American observations, international METAR (Aviation Routine Weather) reports, and the Comprehensive Ocean–Atmosphere Data Set (COADS; Woodruff et al. 1987). Digital satellite imagery from the Space Science and Engineering Center at the University of Wisconsin—Madison was obtained from the University of Utah meteorological archives.

A manually analyzed surface map at 0000 UTC 13 March reveals the atmospheric conditions immediately prior to the development of the gap outflow over the Gulf of Tehuantepec (Fig. 2). At this time, the low center (identified by an L) was located over the northern Gulf of Mexico with the attendant cold front, denoting the

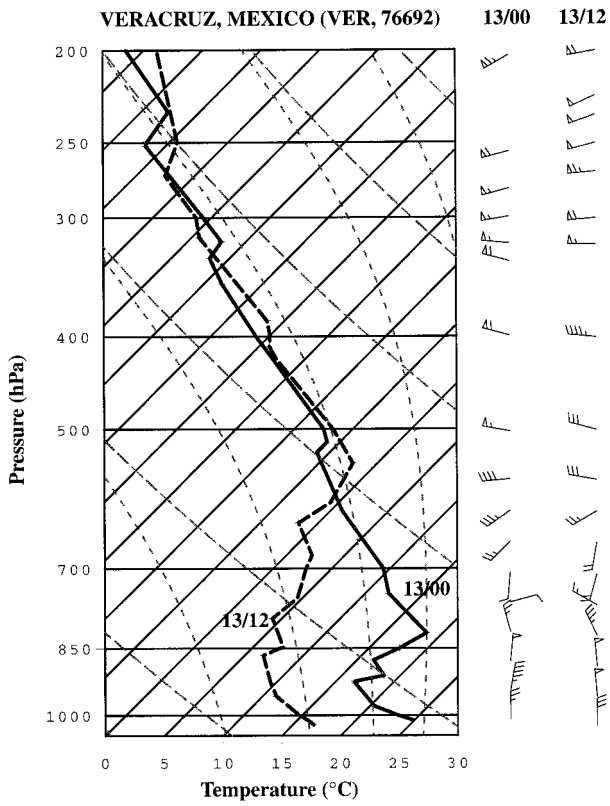

FIG. 3. Temperature and wind profiles from Veracruz, Mexico (VER), at 0000 UTC 13 March and 1200 UTC 13 March. Winds: one pennant, full barb, and half-barb denote 25, 5, and 2.5 m s^{-1}, respectively.

leading edge of the cold surge, extending into southern Mexico just north of Chivela Pass. Behind the cold front, northerly and northwesterly winds were as strong as 20 m s^{-1}. In contrast, coastal stations along the Gulf of Tehuantepec observed southerly or southwesterly winds that appeared to be consistent with the onshore seabreeze circulation that would be expected in the late afternoon (1800 LST). An upper-level sounding from Veracruz (VER) illustrates the vertical structure of the cold surge at 0000 UTC 13 March (Fig. 3). Northerly winds associated with the cold surge extended from the surface to approximately 800 hPa. Above this level, the flow was southerly or westerly. The temperature trace showed a near-surface mixed layer was capped by two stable layers that also reached 800 hPa.

Limited nighttime surface observations prevented detailed analysis for the next several hours. Denser daytime surface observations, timely ship reports, and visible satellite imagery during the following day, however, helped to elucidate the structure of the cold surge and associated gap outflow at 1800 UTC 13 March (Fig. 4). By this time, the cold surge had penetrated equatorward into northeastern Nicaragua and high pressure, with accompanying low clouds, was entrenched along the northern and eastern slopes of the Sierra Madre. The 1200 UTC sounding from VER revealed that a deep layer of cold air was in place upwind of Chivela Pass where a well-mixed surface layer was capped by a series of stable layers that extended to 525 hPa (Fig. 3). With cold air to the north, and an along-gap pressure gradient located over Chivela Pass, Salina Cruz (SCZ) reported 17 m s^{-1} northerly surface winds and a 26°C temperature (Fig. 4a), 3°C colder than 24 h earlier (not shown). Northerly cross-barrier flow was also reported at high-elevation stations east and west of Chivela Pass (Fig. 4a).

Gap outflow extended several hundred kilometers equatorward over the Gulf of Tehuantepec and eastern Pacific Ocean where ships of opportunity reported 15–20 m s^{-1} surface winds (Fig. 4a). At its leading edge, this gap outflow was marked by a line of cumulus convection resembling a rope cloud (Fig. 4b). Isochrones of the rope cloud indicate that the center and western portions turned anticyclonically (westward) as it initially moved over the Pacific Ocean (Fig. 5). Although surface winds behind the cloud band also exhibited anticyclonic curvature (Fig. 4a), it was not possible to determine from the limited observations if the flow traced a path that was consistent with inertial balance. It is also interesting to note that despite the strong northerly flow observed over the Gulf of Tehuantepec, stations located immediately to the west and east of the outflow region were observing winds with a southerly component (Fig. 4a). For example, Tapachula (TAP) reported a southerly wind at 1744 UTC, whereas Bahias de Huatulco (HUX) reported a southwesterly wind at 1545 UTC (observations at 1700 and 1800 UTC were not available). The significance of these observations will be illustrated by the numerical simulation and discussed in section 4.

3. Model description

To understand the mesoscale structure and dynamics of gap outflow over the Gulf of Tehuantepec, a simulation by the nonhydrostatic MM5 (Grell et al. 1994) was used to further examine this event. The simulation featured three domains with horizontal resolutions of 60, 20, and 6.67 km (Fig. 6). The 60- and 20-km domains were two-way nested, allowing for the solution on the 20-km domain to feed back onto the 60-km domain, while the 6.67-km domain was nested in the 20-km domain with a one-way interface. In the vertical, 30 variably spaced half-sigma levels[1] were used for all domains with resolution varying from approximately 10 hPa in the boundary layer to 50 hPa in the upper troposphere. Precipitation processes on all three grids were

[1] The half-sigma levels were located at σ = 0.995, 0.985, 0.970, 0.945, 0.915, 0.885, 0.855, 0.825, 0.795, 0.765, 0.735, 0.705, 0.675, 0.645, 0.615, 0.585, 0.550, 0.510, 0.470, 0.430, 0.390, 0.350, 0.310, 0.270, 0.230, 0.190, 0.150, 0.110, 0.070, 0.025.

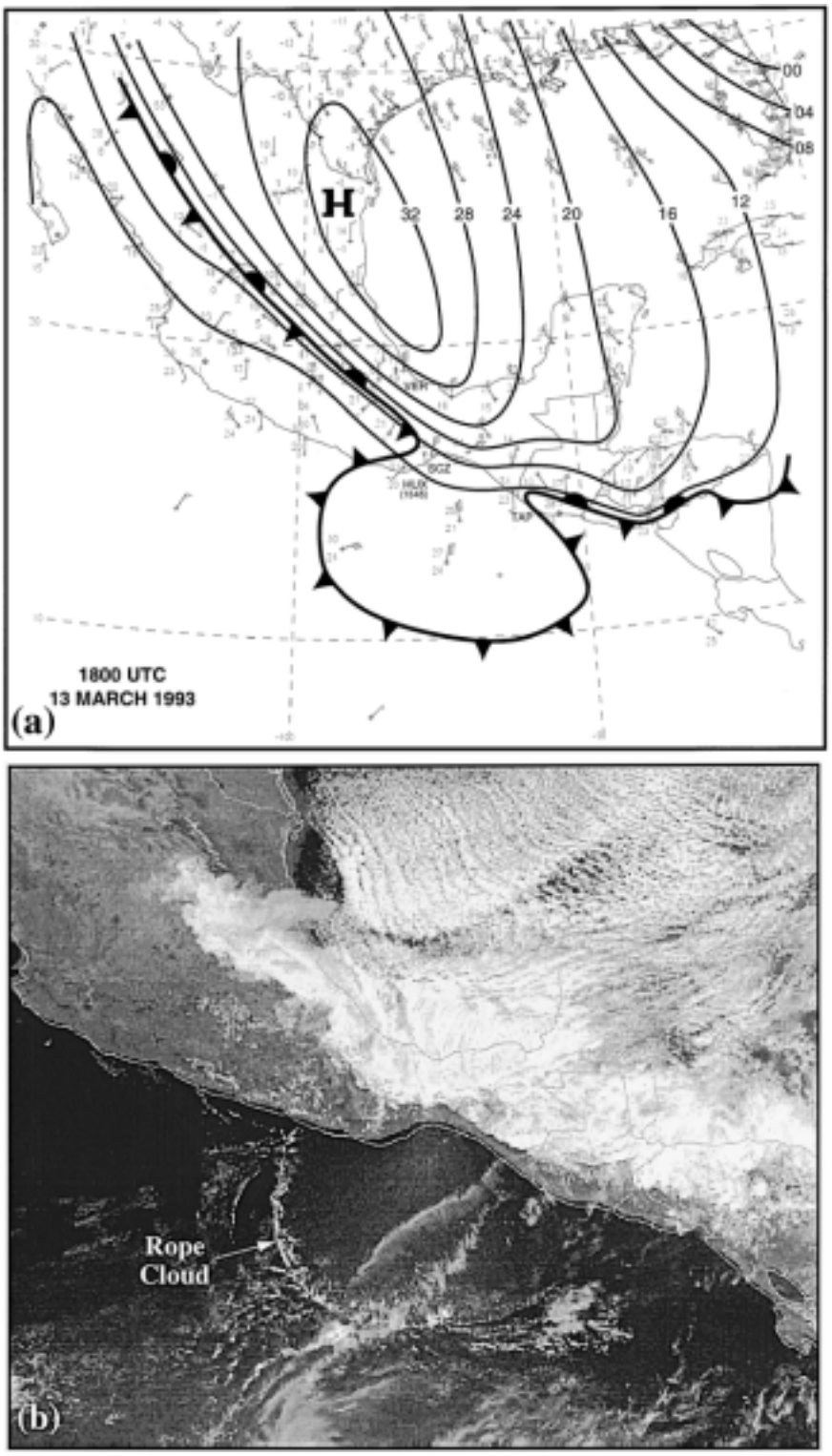

FIG. 4. (a) Manually analyzed surface map at 1800 UTC 13 March (notation as in Fig. 2). (b) *GOES-7* visible satellite imagery at 1801 UTC 13 March.

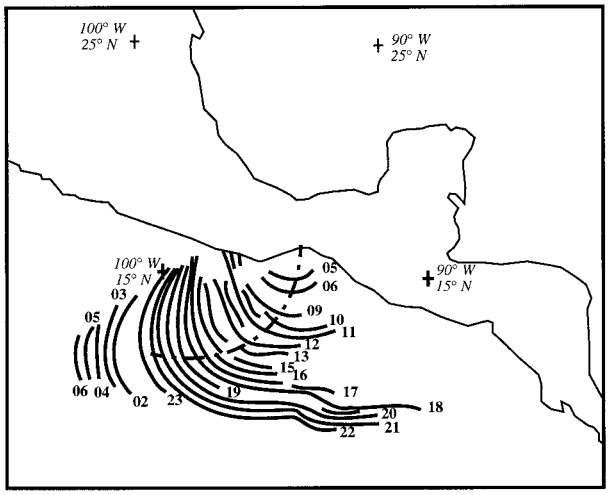

FIG. 5. Isochrones of the cloud band at the leading edge of the gap outflow over the Gulf of Tehuantepec as determined from available visible and infrared satellite imagery for the period from 0500 UTC 13 March to 0600 UTC 14 March. Dash–dot line represents the trajectory of an inertially balanced air parcel with an initial wind speed of 20 m s^{-1} and a radius of curvature of 530 km. Adapted from Schultz et al. (1997).

parameterized using a mixed-phase explicit moisture scheme that includes prognostic equations for water vapor, cloud water, rainwater, cloud ice, and snow and also allows for supercooled water below 0°C. The Kain–Fritsch cumulus parameterization (Kain and Fritsch 1993) was used to represent subgrid-scale convective precipitation for the 60- and 20-km domains. Other parameterizations included a multilayer planetary boundary layer (Zhang and Anthes 1982), a long- and shortwave atmospheric radiation scheme (Dudhia 1989), and a radiative upper boundary condition (Klemp and Durran 1983).

Five-minute averaged terrain, interpolated to the model grid points by a Cressman analysis scheme and filtered by a two-pass smoother/desmoother, provided the model topography (Fig. 6). Analyses from the National Centers for Environmental Prediction, with a 2.5° lat × 2.5° long resolution, were used to generate SST analyses (Fig. 6), except over the Gulf of Mexico where a manually digitized 1° lat × 1° long resolution dataset derived from the operational National Hurricane Center (now known as the Tropical Prediction Center) analysis presented in Gilhousen (1994, his Fig. 10a) was used.

Four-dimensional data assimilation was used to initialize the 60-km and 20-km domains. The assimilation technique employed Newtonian nudging to relax the model simulation to gridded 3-h surface and 12-h upper-level analyses (e.g., Stauffer and Seaman 1990) during a 12-h dynamic-initialization period from 0000 UTC to 1200 UTC 12 March 1993. After this time period, data assimilation was not used. To create 12-h surface and upper-level analyses for the 60- and 20-km domains, analyses from the World Climate Research Programme/Tropical Oceans Global Atmosphere archive I of the European Centre for Medium-Range Weather Forecasts (ECMWF) (Trenberth 1992) were interpolated to the model grids. [These same analyses were used by Schultz et al. (1997)]. Originally stored in spherical harmonic form with an equivalent horizontal latitude–longitude resolution of 1.125°, these analyses were first interpolated to a 1° lat × 1° long grid before interpolation to the mesoscale model grid. Surface and upper-air observations were then incorporated into the analysis using a Cressman-type analysis scheme (Benjamin and Seaman 1985). After the removal of superadiabatic lapse rates below 500 hPa, the analysis was interpolated to sigma coordinates and the integrated mean divergence was removed to avoid the production of spurious gravity waves. Three-hour surface analyses were generated in a similar manner with the first-guess fields derived by linear temporal interpolation of the 12-h ECMWF surface grids. Linear interpolation of the 12-h analyses was also used to provide boundary conditions for the 60-km domain. The 6.67-km domain was initialized at 2100 UTC 12 March 1993 by interpolating simulated model fields from the 20-km domain. The 6.67-km domain was then integrated to 1800 UTC 13 March using boundary conditions provided by hourly output from the 20-km domain.

4. Simulated structure and evolution

Analyses of the structure and evolution of the cold surge and associated gap outflow over the Gulf of Tehuantepec are presented in Figs. 7–12. At 0000 UTC 13 March, the developing low center was located south of Louisiana with a trailing cold front, marking the leading edge of the cold surge, extending into southern Mexico (Fig. 7a). Output from the 6.67-km domain showed that northerlies associated with the cold surge were located just upstream of Chivela Pass (Figs. 8a, 9a). Over the Gulf of Tehuantepec and eastern Pacific, the large-scale pressure gradient was relatively weak (Fig. 8a). Along most of the coast of southern Mexico, an evening sea-breeze circulation was evident and the southerly winds were advecting relatively cool air from over the eastern Pacific into Chivela Pass (Fig. 9a). A north–south-oriented cross section along line AB of Fig. 6 revealed that southerly flow in Chivela Pass extended to about 800 hPa, above which northwesterly flow was moving in aloft (Fig. 10a). This northwesterly flow reached approximately 700 hPa, where winds veered to westerly. Although much of the mesoscale detail of the simulation could not be verified due to limited observations, the contrast in surface winds to the north and south of Chivela Pass appeared to agree well with observations (cf. Figs. 2, 8a).

Over the next 6 h, surface winds in Chivela Pass shifted to northerly as the cold surge moved into the region, and by 0600 UTC 13 March, 15–20 m s^{-1} northerly surface winds extended over the Gulf of Tehuan-

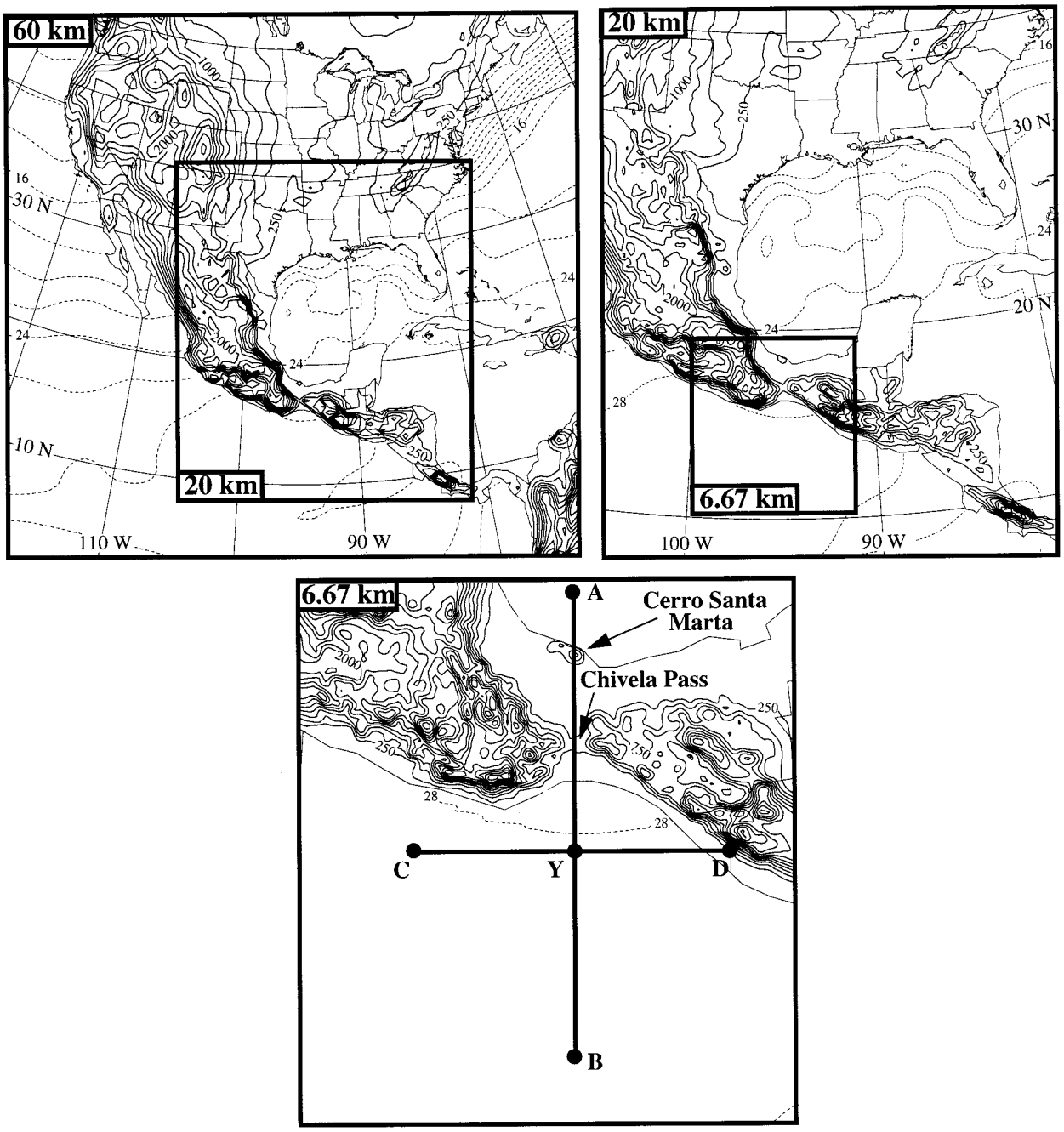

FIG. 6. Model domains, SST (dashed, every 2°C), and topography (solid, every 250 m with the 0-m contour not plotted). Locations of cross sections AB and CD identified with thick solid lines.

tepec (Fig. 8b). This northerly gap outflow was accelerated by an along-gap pressure gradient of approximately 0.75 hPa (10 km)$^{-1}$ that produced a 7.5–10 m s^{-1} increase in wind speed within Chivela Pass. Flow acceleration toward lower pressure continued over the Gulf of Tehuantepec, possibly aided by a decrease in frictional drag as the flow moved over water. Strong northerly flow did not emanate exclusively from Chivela Pass, as the cold surge was able to surmount the relatively low mountains to the east, and, to a lesser extent, to the west of this topographic feature. It is also interesting to note that most of the eastern Pacific developed northerly or northeasterly winds during this period in response to changes in the large-scale pressure field (Fig. 8b).

By 1200 UTC, the simulated low center was located in the southeastern United States and the cold surge had penetrated equatorward to Honduras (Fig. 7b). Winds

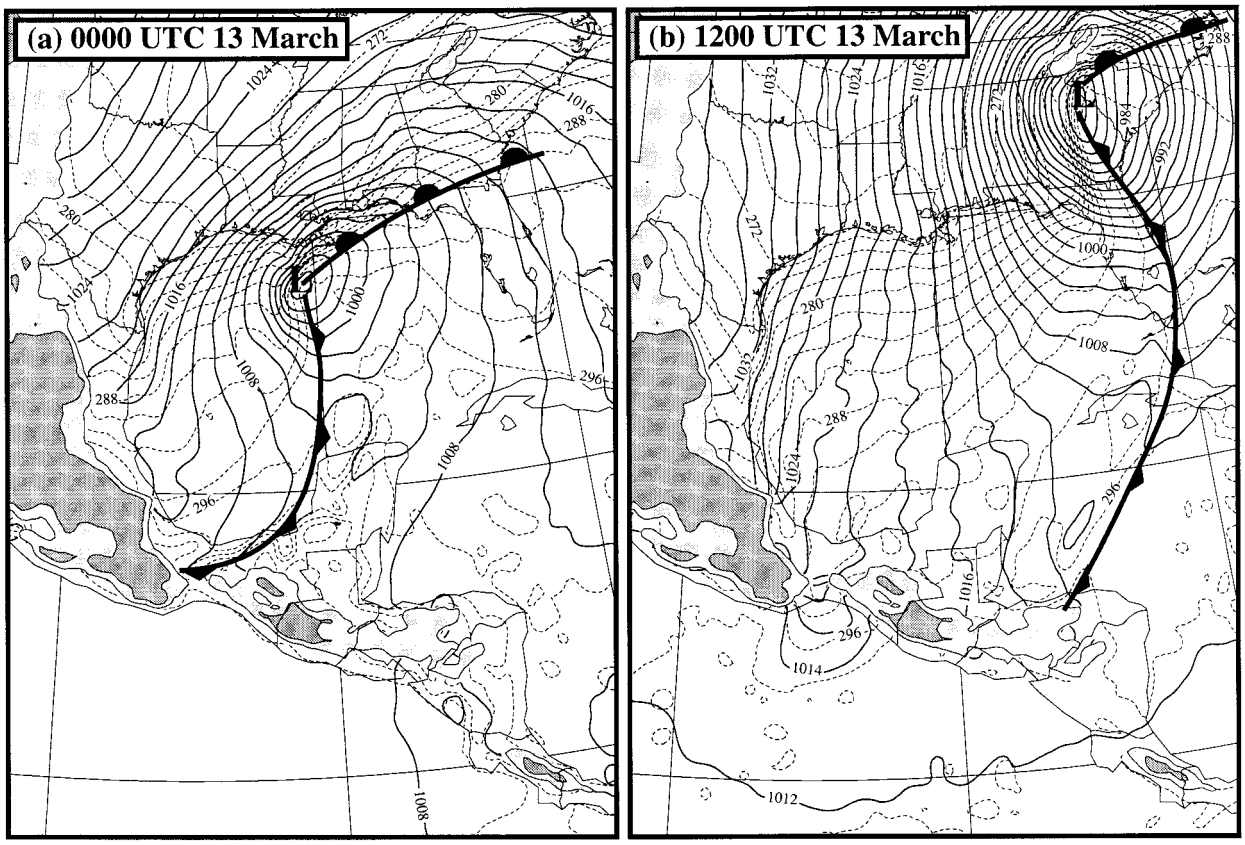

FIG. 7. Simulated sea level pressure (solid, every 2 hPa) and lowest half-sigma level (40 m AGL) potential temperature (dashed, every 2 K) from the 20-km domain at (a) 0000 UTC 13 March and (b) 1200 UTC 13 March. Regions where the model terrain exceeds 750 m (1500 m) are indicated with light (dark) shading. Contours of sea level pressure and potential temperature are not plotted in regions above 750 m in elevation. Conventional frontal notation.

over the Gulf of Tehuantepec intensified to more than 25 m s^{-1} as the along-gap pressure gradient within Chivela Pass increased to almost 1.5 hPa (10 km)$^{-1}$ (Fig. 8c). Strong winds were also evident downwind of the lower mountains surrounding Chivela Pass, particularly those to the east. The flow along and to the west of the jet axis exhibited anticyclonic curvature while to the east of the jet axis the flow became less anticyclonic or even cyclonic (near the Mexico–Guatemala border), resulting in a fanlike wind pattern similar to that described by Trasviña et al. (1995). Strong horizontal shear was evident along the western edge of the outflow jet where an anticyclonic eddy with westerly return flow was evident near the Mexican coast. A weaker cyclonic circulation was also beginning to develop along the eastern edge of the gap outflow near the Mexico–Guatemala border. A mesoscale pressure ridge was located along the outflow-jet axis, with relative minima in pressure associated with the anticyclonic and cyclonic eddies. The strength of the pressure gradient west of the ridge axis was stronger than that to the east. This may have been due to asymmetries in the topography surrounding Chivela Pass, with the relatively high mountains west of the pass more effectively blocking the cold surge and producing stronger lee troughing than the mountains east of the pass. The gap outflow was also associated with a tongue of cold air that extended southward over the Gulf of Tehuantepec and eastern Pacific (Fig. 9b). Compared with the antecedent conditions 12 h earlier (Fig. 9a), surface potential temperatures have dropped as much as 7 K. A strong potential temperature gradient existed along the western edge of the gap outflow near the anticyclonic eddy and a similar, but weaker, gradient was evident to the east.

The development of the mesoscale pressure ridge that was centered along the axis of the outflow jet was associated with the localized movement of relatively cold, dense air over the Gulf of Tehuantepec. A cross section taken across the outflow jet at 1200 UTC (Fig. 11; for position see Fig. 6) showed a layer of relatively cold (i.e., low potential temperature) air that was approximately 200 hPa deep near its center and shallowed toward the flanks of the gap outflow. Using Schoenberger's (1984) formula,

$$\Delta P = (Pg\Delta Z\Delta T_v)/(RT_{vw}T_{vc}), \qquad (2)$$

where ΔP is an estimate of the magnitude of the hydrostatic pressure perturbation beneath the center of the cold dome, P is the environmental pressure (~1010 hPa), g is

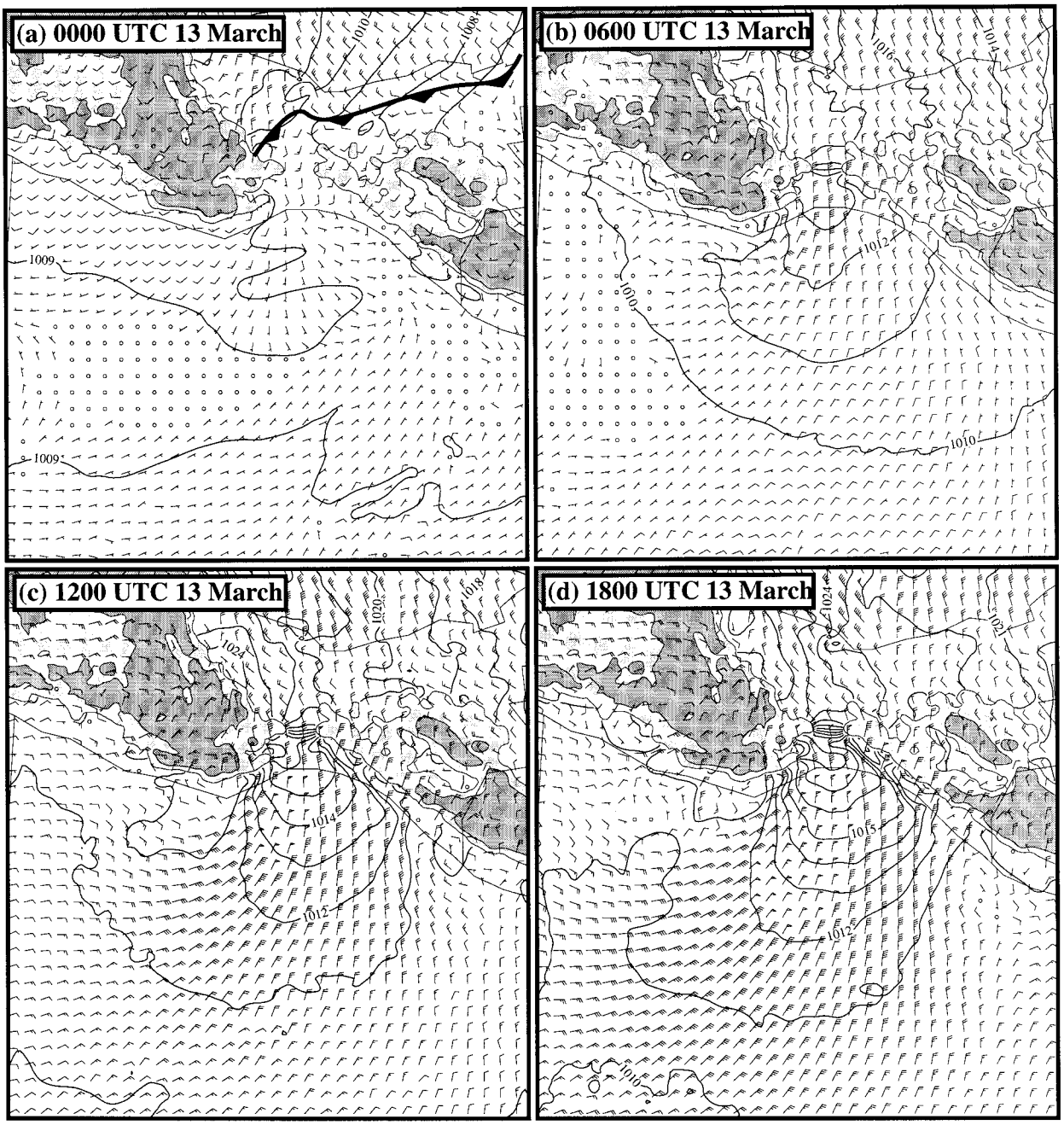

FIG. 8. Simulated sea level pressure (solid, every 1 hPa) and lowest half-sigma level (40 m AGL) winds (one pennant, full barb, half barb, and circle denote 25, 5, 2.5, and less than 1.25 m s^{-1}, respectively) from the 6.67-km domain at (a) 0000 UTC, (b) 0600 UTC, (c) 1200 UTC, and (d) 1800 UTC 13 March. Contours and shading over high terrain as in Fig. 7. Conventional frontal notation in (a).

gravity, ΔZ is the depth of the cold air (~2000 m), R is the gas constant for dry air, T_{vw} is the mean virtual temperature in the warm air (~304 K), T_{vc} is the mean virtual temperature in the cold air (~300 K), and $\Delta T_v = T_{vw} - T_{vc}$, (~4 K), the hydrostatic contribution to higher pressure at the center pressure ridge was estimated to be approximately 3 hPa. This 3-hPa pressure anomaly was consistent with the amplitude of the high-pressure ridge along this cross section (c.f. Figs. 8c and 11).

The north–south-oriented cross section through Chivela Pass (AB) further elucidates the vertical structure of the gap outflow at this time (Fig. 10b). Upwind (north) of Chivela Pass, northwesterly or northerly flow extended from the surface to 700 hPa, above which the flow backed to westerly. This layer of backing winds identified the vertical extent of the cold surge. Over and immediately downwind of Chivela Pass, a wavelike undulation in the isentropes and a region of leeside subsidence were evident,

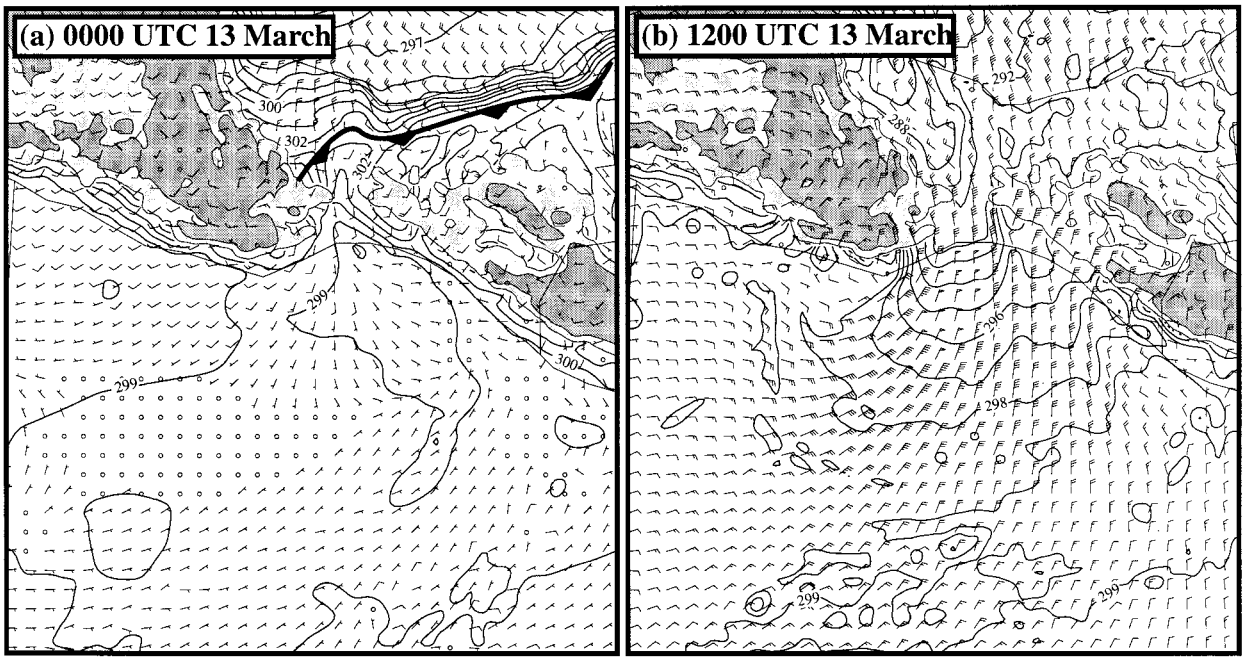

FIG. 9. Simulated lowest half-sigma level (40 m AGL) potential temperature (solid, every 1 K) and winds (one pennant, full barb, half barb, and circle denote 25, 5, 2.5, and less than 1.25 m s^{-1}, respectively) at (a) 0000 UTC 13 March and (b) 1200 UTC 13 March. Contours and shading over high terrain as in Fig. 7. Conventional frontal notation in (a).

suggesting that this relatively low topographic feature has excited a mountain wave (e.g., Durran 1986, 1990). Larger-amplitude mountain waves were also found east of Chivela Pass (not shown) where northerly flow was able to surmount the Sierra Madre, accelerate rapidly over the lee slopes, and extend over the Gulf of Tehuantepec (Fig. 8c). The cross section and a model-derived sounding (Fig. 12; for position see Fig. 6) also illustrate the vertical stratification in the outflow region. At low levels, a 75-hPa-deep surface-based mixed layer, which likely was produced by surface sensible heating and boundary layer mixing over the Gulf of Tehuantepec, was capped by a near-isothermal layer that reached 875 hPa. The strongest northerly winds, with magnitudes as high as 25–30 m s^{-1}, were found in these layers. Further aloft, winds veered and weakened with height through a layer of weaker static stability (875–800 hPa) that was capped by a stable layer that extended to near 725 hPa. Ambient southwesterly to northwesterly flow was found above this level. Similar multilayered flow was found in a numerical study of gap outflow from Howe Sound, British Columbia (Jackson and Steyn 1994a).

Changes in surface friction appeared to have a major impact on surface winds as they moved from the land to over the Gulf of Tehuantepec. As shown in Fig. 10b, surface winds were weaker and surface-to-900-hPa wind shear was stronger immediately downwind of Chivela Pass than over the Gulf of Tehuantepec. This appeared to be due to a decrease in frictional drag as the flow moved over the gulf.

Figure 8d presents the simulated sea level pressure and lowest half-sigma level winds at 1800 UTC 13 March, which can be compared to surface observations presented in Fig. 4a. The numerical simulation appears to capture the general character of this event. For example, the 17.5 m s^{-1} northerly wind at Salina Cruz (SCZ), immediately downwind of Chivela Pass, agrees well with the 20 m s^{-1} northerly wind produced by the simulation. Simulated winds (Fig. 8d) also closely match the three ship reports over the Gulf of Tehuantepec (Fig. 4a), although the simulated winds are approximately 20% stronger than those observed. This discrepancy is produced, in part, by the fact that the model's lowest half-sigma level winds are located at 40 m above ground level (AGL), while the reported winds were likely observed at a lower level (e.g., 10 m). The model may also be underestimating the impact of ocean wave activity on surface roughness. The fanning of winds over the gulf appears to be similar to that observed in other events by Barton et al. (1993) and Trasviña et al. (1995), and the development of reversed flow along the coastlines is suggested by the observed winds at TAP and HUX (cf. Figs. 4a, 8d). The structure of the gap outflow has changed little over the previous 6 h except for a slight increase in the strengths of the pressure gradient and surface winds over the Gulf (cf. Figs. 8c,d).

5. Trajectory and momentum-balance diagnostics

a. General airflow

Three-dimensional trajectories, beginning at 0000 UTC 13 March and terminating on the model's lowest

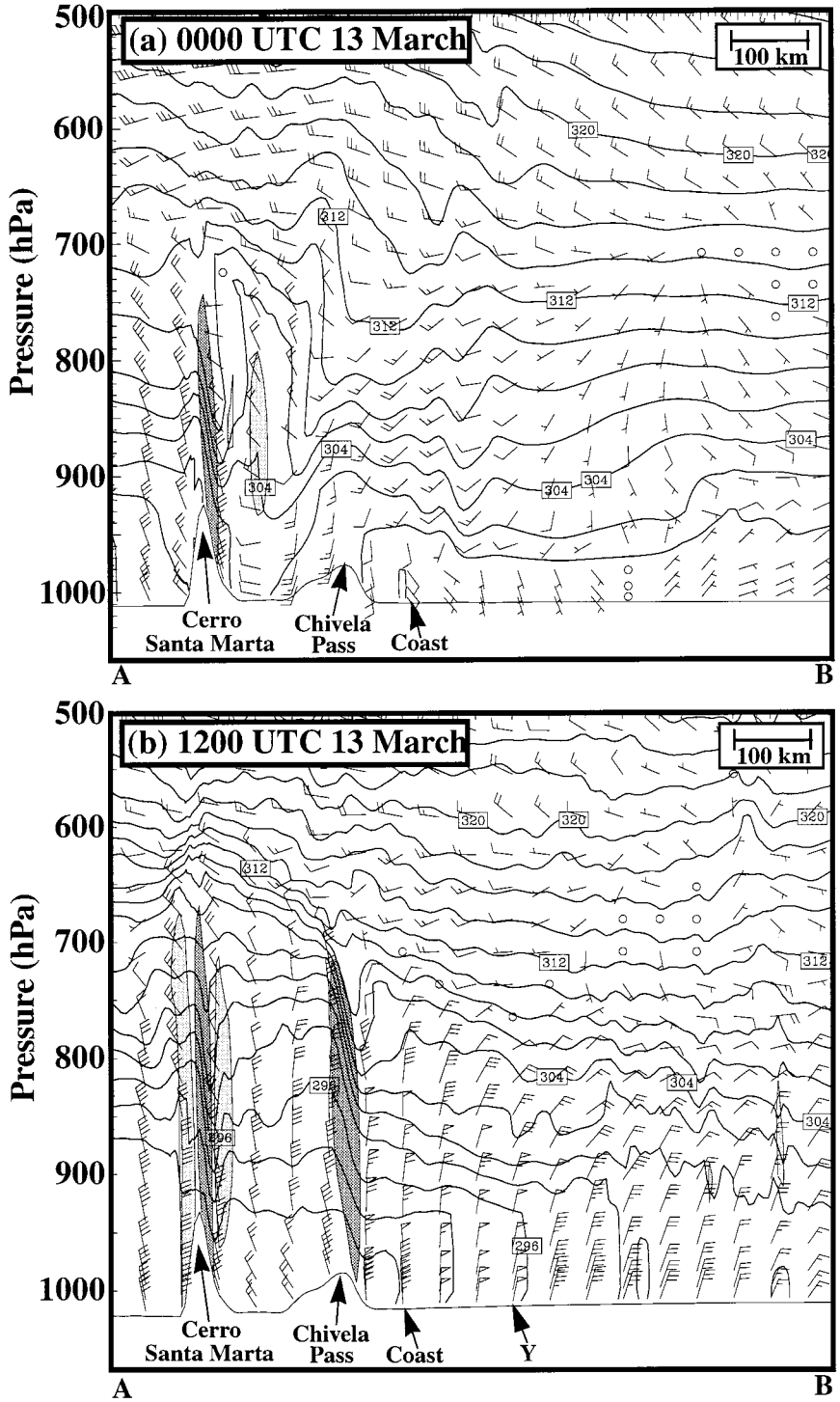

FIG. 10. Cross sections of potential temperature (every 2 K) and horizontal wind along line AB of Fig. 6 at (a) 0000 UTC and (b) 1200 UTC 13 March. One pennant, full barb, half barb, and circle denote 25, 5, 2.5, and less than 1.25 m s^{-1}, respectively. Wind barbs oriented so north is toward the top of the page. Light (dark) shading identifies regions of rising (sinking) motion exceeding 3×10^{-1} m s^{-1} in magnitude.

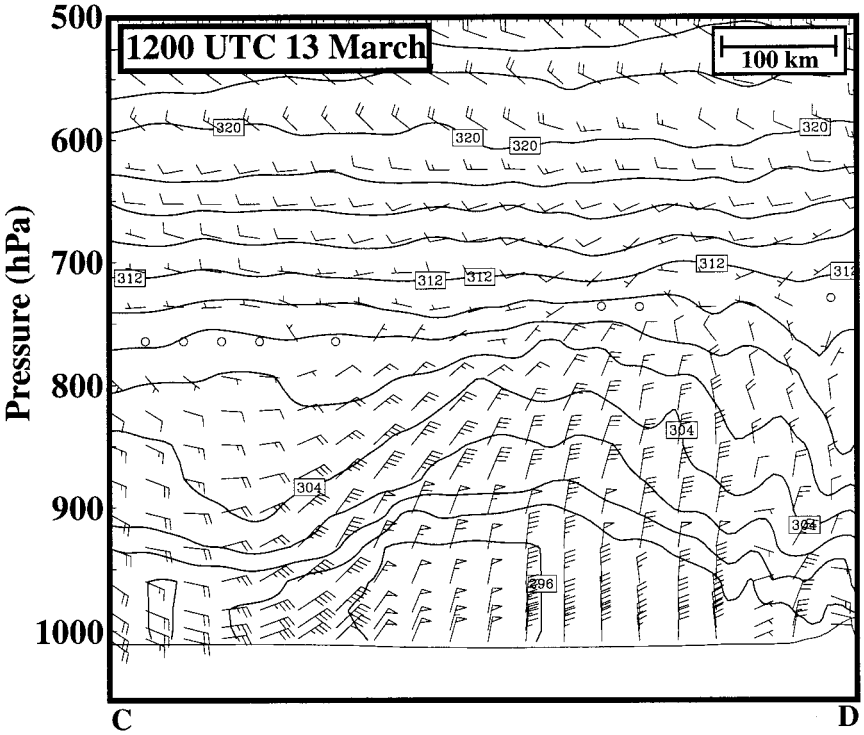

FIG. 11. Cross section of potential temperature (every 2 K) and horizontal wind along line CD of Fig. 6 at 1200 UTC 13 March. One pennant, full barb, half barb, and circle denote 25, 5, 2.5, and less than 1.25 m s^{-1}, respectively. Wind barbs oriented so north is toward the top of the page.

half-sigma level [approximately 40 m above ground AGL] at 1200 UTC 13 March, elucidate the low-level airflow over Chivela Pass, the Gulf of Tehuantepec, and surrounding region after passage of the leading edge of the cold surge (Fig. 13). Trajectories 4, 5, and 6 were strongly accelerated as they moved through and downstream of Chivela Pass, and then turned anticyclonically over the Gulf of Tehuantepec. For example, the speed of trajectory 5 was initially 10 m s^{-1}, but increased to approximately 20 m s^{-1} within Chivela Pass (Fig. 14). Flow acceleration then continued over the Gulf of Tehuantepec until the speed of trajectory 5 reached a maximum of 24.3 m s^{-1} at 1100 UTC 13 March (Fig. 14). Over the Gulf of Tehuantepec, the radii of curvature for these trajectories closely matched that for inertially balanced flow (580 km; heavy dashed line in Fig. 13), assuming a wind speed of 22 m s^{-1} and a latitude of 15°N. In fact, the 580-km inertial radius of curvature falls between the radii of curvature of trajectories 5 and 6.

Trajectories to the west of the outflow-jet axis exhibited stronger anticyclonic curvature than predicted by inertial balance (Fig. 13). Trajectory 1 originated over the Sierra Madre, descended over the Gulf of Tehuantepec, and turned sharply anticyclonically. Eventually this trajectory encircled the anticyclonic eddy and pressure minimum that were located to the lee of the high terrain west of Chivela Pass (Fig. 8c). Trajectories 2 and 3 originated from north and east of the Sierra Madre, ascended moderate-elevation terrain immediately west of Chivela Pass, descended, and moved over the Gulf of Tehuantepec (Fig. 13). Trajectories 7–10, located east of the outflow-jet axis, were characterized by relatively straight or cyclonically curved paths. These trajectories originated at relatively low elevations near the Bay of Campeché and were able to ascend the mountains east of Chivela Pass before descending and moving rapidly over the Gulf of Tehuantepec. These trajectories show that the movement of cold air across the Sierra Madre is not necessarily confined to Chivela Pass, but may also occur over the relatively low mountains east, and to a lesser extent west, of the pass. In summary, although trajectories near the center of the outflow jet appear to follow paths consistent with an inertial balance, surrounding trajectories do not necessarily follow such paths. Trajectories to the west of the outflow jet experienced stronger anticyclonic curvature, while those to the east followed paths that were straight or curved cyclonically. This fanlike flow pattern will be explained in the next section.

b. Momentum balance and comparison to inertial flow

To understand the dynamics of flow curvature during this gap-outflow event, terms of the MM5 horizontal momentum tendency equations [Grell et al. 1994, Eqs.

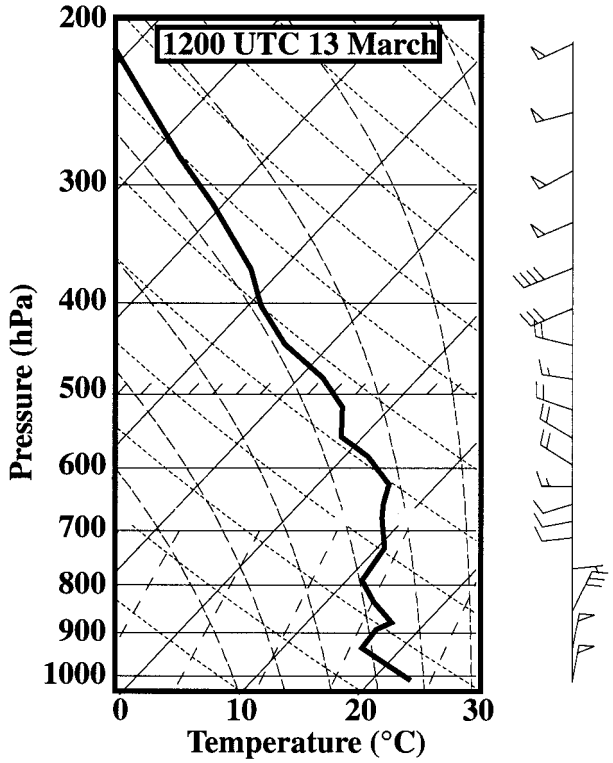

FIG. 12. Simulated temperature and wind profiles at point Y of Figs. 6 and 10b at 1200 UTC 13 March. Pennant, full barb, and half barb denote 25, 5, and 2.5 m s^{-1}, respectively.

(2.2.1) and (2.2.2)] were output during the model simulation and then evaluated along trajectories over the Gulf of Tehuantepec. Because the MM5 horizontal momentum tendency equations are expressed in flux form, these terms were converted into their more traditional primitive-equation formulations, resulting in a momentum equation that can be summarized as

$$\frac{d\mathbf{V}}{dt} = -\frac{1}{\rho}\nabla p - f\hat{\mathbf{k}} \times \mathbf{V} + \text{residual}, \qquad (3)$$

where d/dt is the total derivative with respect to time (composed of the local time tendency and the horizontal and vertical advection terms) and V is the horizontal velocity vector. The first two terms on the right-hand side represent the pressure-gradient and Coriolis accelerations and ''residual'' is the residual acceleration, which includes the effects of diffusion, parameterized boundary layer processes, and numerical truncation errors. Using this equation, the cross- and along-flow momentum balance following selected trajectories was then evaluated. The cross-flow momentum balance was used to examine factors producing flow curvature, while the along-flow momentum balance was used to diagnose changes in wind speed. In the case of inertial flow, the horizontal pressure-gradient acceleration is negligible, flow curvature is produced by the Coriolis acceleration, and there is no net acceleration in the along-flow direction. The latter can occur for frictionless flow if there is a uniform pressure or geopotential height field (Holton 1992, 64–65).

The cross-flow momentum balance along three selected outflow trajectories is displayed in Fig. 15, with the cross-flow component of the Lagrangian parcel ($d\mathbf{V}/dt$), pressure-gradient, Coriolis, and residual accelerations labeled L, PG, C, and R, respectively. After 1000 UTC 13 March, trajectory 11, which followed the axis of the outflow jet and mesoscale pressure ridge, exhibited anticyclonic curvature that was produced primarily by the Coriolis acceleration. Except for 1000 UTC 13 March, when a significant cross-flow pressure-gradient acceleration was observed,[2] the cross-flow pressure-gradient acceleration along this trajectory was negligible and the trajectory traced a path that was consistent with inertial balance.

The along-flow momentum balance following trajectory 11 is displayed in Fig. 16. Although a significant along-flow pressure-gradient acceleration existed along this trajectory, it was countered by the residual acceleration, which was presumably dominated by frictional effects. As a result, the net along-flow Lagrangian parcel acceleration at 1000 and 1100 UTC 13 March was negligible and the trajectory exhibited inertial balance. By 1200 UTC 13 March, the along-flow pressure gradient had weakened and the flow was beginning to decelerate.

Although trajectories along the axis of the outflow jet were inertially balanced, the momentum balances along trajectories surrounding the axis of the outflow jet were modified by cross-flow pressure-gradient accelerations (Fig. 15). Trajectories on the anticyclonic side of the jet axis, such as trajectory 3, experienced stronger anticyclonic curvature than expected from inertial balance because the cross-flow pressure-gradient acceleration resulted in a net acceleration that was stronger than that produced solely by the Coriolis acceleration. In contrast, trajectories on the cyclonic side of the jet axis exhibited weaker anticyclonic curvature or followed straight paths because the cross-flow pressure-gradient acceleration was directed opposite the Coriolis acceleration. For example, trajectory 8 followed a relatively straight path because the cross-flow pressure-gradient acceleration nearly balanced the Coriolis and residual accelerations. Because of the influence of these cross-flow pressure-gradient accelerations on trajectories surrounding the jet axis, the flow fanned out in the outflow region rather than maintaining a narrow jet as one might expect based on the scale analysis of Clarke (1988), which assumed a negligible pressure gradient over the gulf.

[2] The cross-flow pressure-gradient acceleration at this time was produced by transient pressure fluctuations rather than the steady mesoscale pressure field.

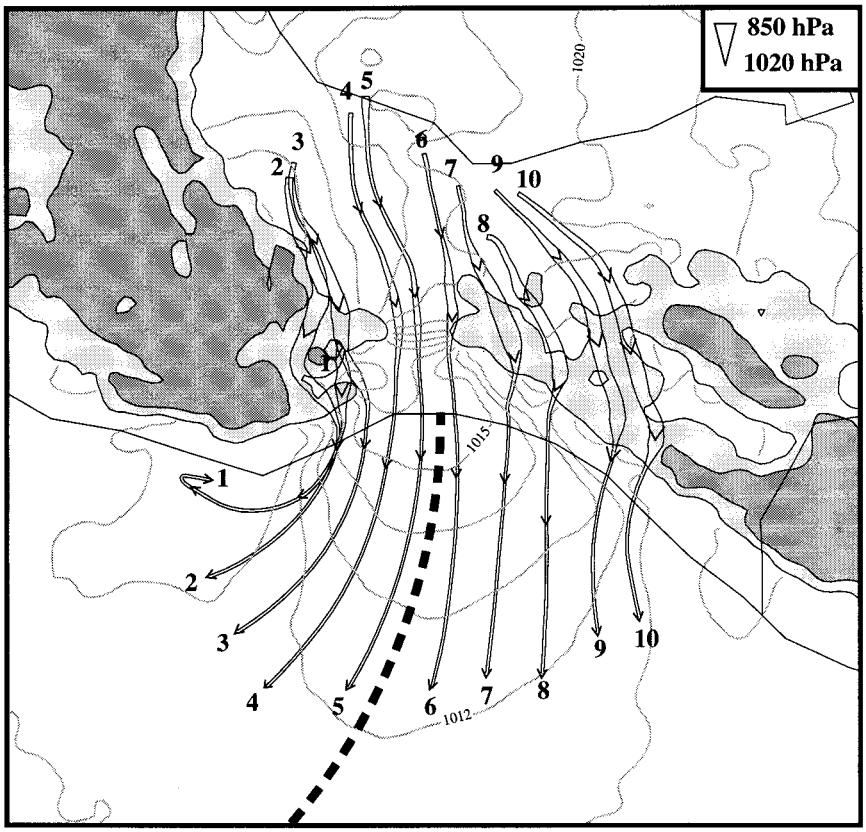

FIG. 13. Twelve-hour three-dimensional trajectories beginning at 0000 UTC 13 March and ending on the model's lowest half-sigma level (40 m AGL) at 1200 UTC 13 March. Sea level pressure contours (light gray) every 1 hPa. Terrain shading as in Fig. 7. Arrows along trajectory paths denote trajectory positions at 0300 UTC, 0600 UTC, 0900 UTC, and 1200 UTC 13 March. Thick dashed line represents an inertial-path radius of 580 km, corresponding to a wind speed of 22 m s^{-1} and latitude of 15°N.

c. Downstream extension of gap outflow

A unique characteristic of gap-outflow winds over the Gulf of Tehuantepec, as well as the Gulfs of Fonseca, Papagayo, and Panama, is that they occasionally extend several hundred kilometers over the eastern Pacific (e.g., Parmenter 1970; Stumpf 1975b; Legeckis 1988; Schultz et al. 1997). Yet most other studies suggest that outflow from other gaps often weakens or merges with the ambient flow in just a few tens of kilometers (e.g., Overland and Walter 1981; Bond and Macklin 1993). Possible reasons for this discrepancy include the following:

1) Weak synoptic-scale forcing (i.e., surface pressure gradients and winds) over the Gulf of Tehuantepec during gap-outflow events. As a result, winds emerging from Chivela Pass are not forced to merge rapidly with the ambient synoptic-scale flow.
2) A lack of terrain features in the Gulf of Tehuantepec. Many areas in which strong gap winds occur are also characterized by relatively complex topography in the outflow region [e.g., Howe Sound (Jackson and Steyn 1994a,b), Fraser River Valley (Mass et al. 1995)]. In contrast, outflow from Chivela Pass moves over an oceanic region with no terrain features.
3) The relatively small Coriolis parameter at the Gulf of Tehuantepec (15°N). For a given wind speed, an inertially balanced trajectory at 45°N would have a radius of curvature approximately 2.7 times smaller than it would over the Gulf of Tehuantepec. Thus, outflow at higher latitudes would exhibit more pronounced curvature and less extension away from the gap. To illustrate the effect of the Coriolis parameter, two sensitivity studies were run in which the Coriolis parameter in the 6.67-km domain was set to constant values corresponding to 45°N ($f = 1.03 \times 10^{-4}\ s^{-1}$, Fig. 17a) and 0° ($f = 0\ s^{-1}$, Fig. 17b). Compared to the control simulation (Fig. 8c), the outflow in the 45°N simulation (Fig. 17a) exhibited stronger anticyclonic deflection and wind speeds decreased more rapidly as one moved equatorward from the gap. The 0° simulation (Fig. 17b) produced less curvature and the fanning of the flow was more symmetric than either the control or 45°N simulations.

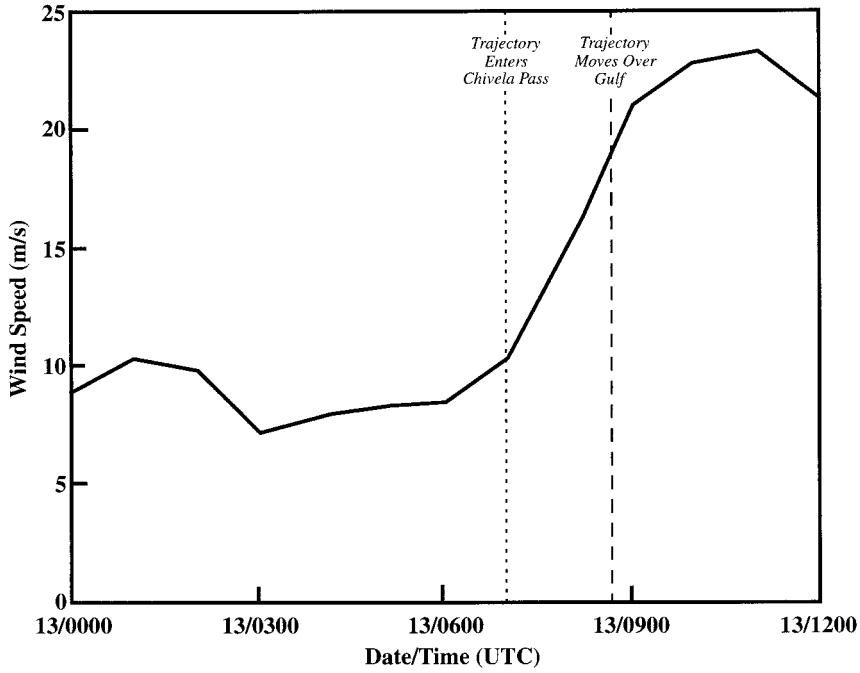

FIG. 14. Wind speed along trajectory 5 of Fig. 13. Dotted line identifies the time the trajectory entered Chivela Pass, whereas the dashed line identifies the time the trajectory moved over the Gulf of Tehuantepec.

6. Summary and future directions

Using output from a high-resolution mesoscale model, this paper has examined the structure and dynamics of a gap-outflow event over the Gulf of Tehuantepec, Mexico. The event was associated with the Central American cold surge of 12–14 March 1993, which established relatively high pressure over the Gulf of Mexico and Bay of Campeché, producing gap winds in Chivela Pass, a low-elevation gap in the Sierra Madre. Simulated gap-outflow winds emerged in a low-level jet from Chivela Pass, reached a maximum speed at the surface of $\sim$25 m s^{-1}, and turned anticyclonically while fanning out over the gulf. Strong northerly winds over the Gulf of Tehuantepec also occurred to the lee of the relatively low mountains east, and to a lesser extent west, of Chivela Pass, indicating that the movement of cold air across the Sierra Madre was not confined to the pass. The resulting fanlike wind pattern closely resembled that observed in similar gap-outflow events (e.g., Barton et al. 1993; Trasviña et al. 1995) rather than a narrow and confined jet, as might be inferred from scale analysis assuming a negligible pressure gradient downwind of the gap (e.g., Clarke 1988). The outflow was also flanked by anticyclonic and cyclonic eddies, with the anticyclonic eddy exhibiting a stronger circulation than the cyclonic eddy.

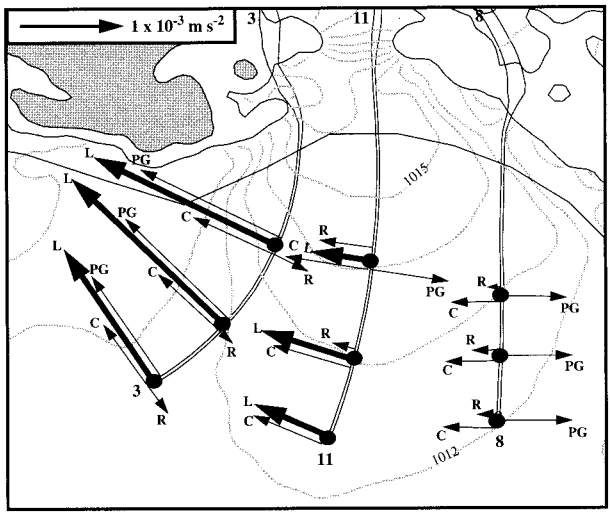

FIG. 15. Cross-flow momentum balance at 1000 UTC, 1100 UTC, and 1200 UTC 13 March along three-dimensional trajectories ending on the model's lowest half-sigma level (40 m AGL) at 1200 UTC 13 March. Cross-flow Lagrangian parcel (bold), pressure gradient, Coriolis, and residual acceleration vectors labeled as L, PG, C, and R, respectively. Vector scale as indicated in the inset at upper left with vectors of negligible magnitude not plotted. Sea level pressure contours at 1200 UTC 13 March (light gray, every 1 hPa).

Model-derived momentum balances were used to examine the dynamics of flow curvature over the Gulf of Tehuantepec. Along a trajectory that followed the axis of the outflow jet, the cross-flow pressure-gradient acceleration was negligible and anticyclonic flow curvature was produced primarily by the Coriolis acceleration, as would be expected from inertial balance. Trajectories to the west of the outflow jet, however, ex-

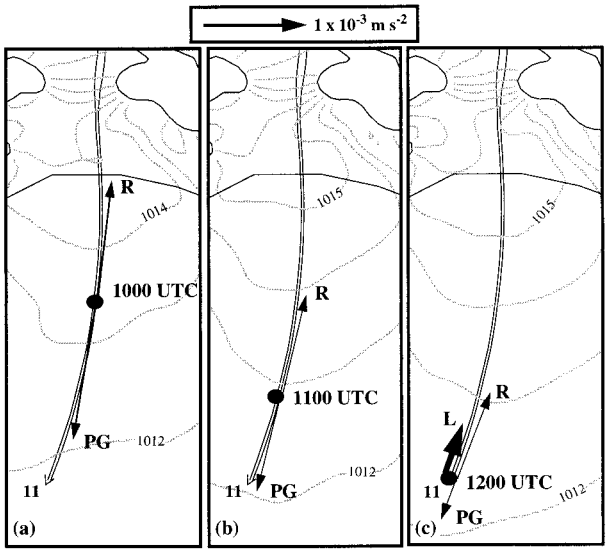

FIG. 16. Sea level pressure analysis (light gray every 1 hPa) and along-flow momentum balance following trajectory 11 at (a) 1000 UTC, (b) 1100 UTC, and (c) 1200 UTC 13 March. Along-flow Lagrangian parcel (bold), pressure gradient, and residual acceleration vectors labeled L, PG, and R, respectively. Vector scale as indicated in the inset at top. The Coriolis acceleration vector at all times and the Lagrangian parcel acceleration vector at 1000 and 1100 UTC are of negligible magnitude and are not plotted.

perienced stronger anticyclonic flow curvature than predicted by inertial balance. This enhanced flow curvature was produced by a cross-flow pressure-gradient acceleration that acted in the same direction as the Coriolis acceleration and was associated with a mesoscale pressure ridge that was aligned along the axis of the outflow jet. In contrast, trajectories to the east of the jet axis exhibited weaker anticyclonic curvature or followed relatively straight or cyclonic paths because the cross-flow pressure-gradient acceleration was directed opposite the Coriolis acceleration. These cross-flow pressure-gradient accelerations produced the fanlike wind pattern over the Gulf of Tehuantepec. In addition, the cross-flow pressure gradient on the anticyclonic side of the jet was considerably stronger than on the cyclonic side of the jet. This asymmetrical pressure pattern may have been the result of the local terrain characteristics, with the relatively high mountains west of the pass more effectively blocking the cold surge and producing stronger lee troughing than the lower mountains east of the pass.

Further refinement of mesoscale-model simulations of these events may be possible by improving the representation of SST and surface roughness. As noted in section 1, gap outflow over the Gulf of Tehuantepec can produce a lowering of SST as large as 8°C within a few hours. Such SST tendencies were not included in the present simulation, which featured fixed SSTs (~28°C) over the Gulf of Tehuantepec (Fig. 6). In addition, the surface roughness length over water was parameterized

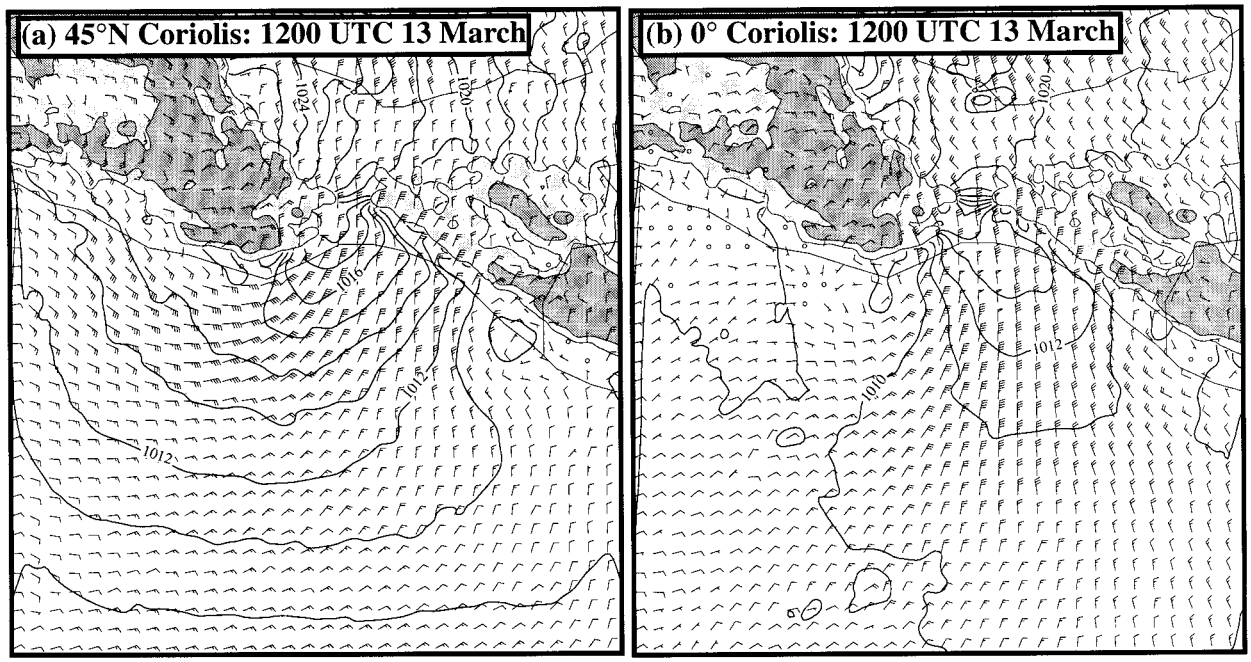

FIG. 17. Simulated sea level pressure (solid, every 1 hPa) and lowest half-sigma level (40 m AGL) winds at 1200 UTC 13 March from 6.67-km domain sensitivity studies with the Coriolis parameter set to values at (a) 45°N and (b) 0°. One pennant, full barb, half-barb, and circle denote 25, 5, 2.5, and less than 1.25 m s^{-1}, respectively. Contours and shading over high terrain as in Fig. 7.

as a relatively simple function of friction velocity [Grell et al. 1994, Eq. (5.4.3.16)], which can underestimate surface roughness length during periods of strong winds and ocean wave activity (Powers 1996). Coupling the atmospheric model with an ocean circulation and surface wave model (e.g., Doyle 1995; Powers 1996; Hodur 1997) may improve the representation of surface heat, moisture, and momentum fluxes. In such coupled systems, the atmospheric model provides momentum- and heat-flux information to the ocean circulation and surface wave models, which, in turn, provide surface characteristics for the atmospheric model including SST and information concerning wave height and phase velocity. Based on the preliminary findings of Powers (1996), who examined the passage of a cold front over Lake Erie, we speculate that this air–sea coupling would improve the simulated modification of boundary layer temperatures as the cold surge moves over the Gulf of Tehuantepec. The strength of the outflow jet near the surface may also be reduced compared to that predicted by our uncoupled simulation because of the increased surface roughness length. Such model improvements will also require more detailed observational datasets of these events for model validation, including measurements of surface flux and sea-state characteristics.

A coupled atmosphere–ocean mesoscale simulation could also help improve understanding of the oceanographic response to the gap outflow, which, in addition to the dramatic changes in SST, also includes the development of an anticyclonic oceanic eddy in the western Gulf of Tehuantepec and a weaker, cyclonic oceanic eddy in the eastern gulf (Barton et al. 1993; Trasviña et al. 1995). Previous modeling of the oceanic response during these wind events has typically assumed relatively simple and steady-state wind forcing. For example, McCreary et al. (1989) used a 400-km long, 280-km wide, straight wind jet without the observed fanlike spreading of the wind, whereas Trasviña Castro (1991) utilized a spreading Gaussian jet. Neither simulation considered the anticyclonic curvature of the jet or the flanking anticyclonic and cyclonic atmospheric eddies that were present in the MM5 simulation, which could play a role in the development of the oceanic eddies. A coupled atmosphere–ocean mesoscale model could also be used to examine relationships, similar to those hypothesized by Schultz et al. (1998), between intra- and interseasonal variability in Central American cold surges, upwelling and SST anomalies over the Gulf of Tehuantepec and eastern Pacific, and the El Nino–Southern Oscillation.

Acknowledgments. This work was conducted with support provided to the first author by National Science Foundation Grant ATM-9634191 and NOAA Grant OGP-526404 and while the second author was a National Research Council postdoctoral research associate at the National Severe Storms Laboratory. We are grateful to the University of Utah Center for High Performance Computing, ECMWF, and the Data Support Section of the Scientific Computing Division of NCAR for providing data and a portion of the computer resources used in this study. Special thanks to Lance Bosart, Ed Bracken, Chuck Doswell, John Horel, Haig Iskenderian, Dan Keyser, Gary Lackmann, Jan Paegle, Jordan Powers, Mark Stoelinga, and three anonymous reviewers for their contributions, advice, and scientific support. Thanks also to Joan O'Bannon, who drafted Figs. 2 and 4a.

REFERENCES

Barton, E. D., and Coauthors, 1993: Supersquirt: Dynamics of the Gulf of Tehuantepec, Mexico. *Oceanography,* **6,** 23–30.

Benjamin, S. G., and N. L. Seaman, 1985: A simple scheme for objective analysis in curved flow. *Mon. Wea. Rev.,* **113,** 1184–1198.

Bond, N. A., and S. A. Macklin, 1993: Aircraft observations of offshore-directed flow near Wide Bay, Alaska. *Mon. Wea. Rev.,* **121,** 150–161.

Bosart, L. F., G. J. Hakim, K. R. Tyle, M. A. Bedrick, W. E. Bracken, M. J. Dickinson, and D. M. Schultz, 1996: Large-scale antecedent conditions associated with the 12–14 March 1993 cyclone (''Superstorm '93'') over eastern North America. *Mon. Wea. Rev.,* **124,** 1865–1891.

Cameron, D. C., 1931: Easterly gales in the Columbia River Gorge during the winter of 1930–1931—Some of their causes and effects. *Mon. Wea. Rev.,* **59,** 411–413.

——, and A. B. Carpenter, 1936: Destructive easterly gales in the Columbia River Gorge, December 1935. *Mon. Wea. Rev.,* **64,** 263–267.

Caplan, P. M., 1995: The 12–14 March 1993 Superstorm: Performance of the NMC global medium-range model. *Bull. Amer. Meteor. Soc.,* **76,** 201–212.

Clarke, A. J., 1988: Inertial wind path and sea surface temperature patterns near the Gulf of Tehuantepec and Gulf of Papagayo. *J. Geophys. Res.,* **93,** 15 491–15 501.

Decker, F. W., 1979: Oregon's silver thaw. *Weatherwise,* **32,** 76–78.

Dickinson, M. J., L. F. Bosart, W. E. Bracken, G. J. Hakim, D. M. Schultz, M. A. Bedrick, and K. R. Tyle, 1997: The March 1993 Superstorm cyclogenesis: Incipient phase synoptic- and convective-scale flow interaction and model performance. *Mon. Wea. Rev.,* **125,** 3041–3072.

Dorman, C. E., R. C. Beardsley, and R. Limeburner, 1995: Winds in the Strait of Gibraltar. *Quart. J. Roy. Meteor. Soc.,* **121,** 1903–1921.

Doyle, J. D., 1995: Coupled ocean wave/atmosphere mesoscale models of cyclogenesis. *Tellus,* **47A,** 766–778.

Dudhia, J., 1989: Numerical study of convection observed during the Winter Monsoon Experiment using a mesoscale two-dimensional model. *J. Atmos. Sci.,* **46,** 3077–3107.

Durran, D. R., 1986: Mountain waves. *Mesoscale Meteorology and Forecasting,* P. Ray, Ed., Amer. Meteor. Soc., 472–492.

——, 1990: Mountain waves and downslope winds. *Atmospheric Processes over Complex Terrain,* W. Blumen, Ed., Amer. Meteor. Soc., 59–81.

Fiedler, P. C., 1994: Seasonal and interannual variability of coastal zone color scanner phytoplankton pigments and winds in the eastern tropical Pacific. *J. Geophys. Res.,* **99,** 18 371–18 384.

García, S. O., and S. Lluch-Cota, 1996a: Distribución de la abundancia de atún aleta amarilla (*Thunnus albacares*) y su relación con la concentración de pigmentos fotosintéticos medidos por satélite en aguas al sur de México. *Invest. Geogr. Bol.,* **4,** 85–93.

——, and ——, 1996b: Relative abundance of yellowfin tuna distributions relative to environmental features observed from satellites. *Tuna Newsl.,* **122,** 5.

Gilhousen, D. B., 1994: The value of NDBC observations during March 1993's ''Storm of the Century.'' *Wea. Forecasting,* **9,** 255–264.

Grell, G. A., J. Dudhia, and D. R. Stauffer, 1994: A description of the fifth-generation Penn State/NCAR Mesoscale Model (MM5). NCAR Tech. Note NCAR/TN-398+STR, 138 pp. [Available from UCAR Communications, P.O. Box 3000, Boulder, CO 80307.]

Hodur, R. M., 1997: The Naval Research Laboratory's Coupled Ocean–Atmosphere Mesoscale Prediction System (COAMPS). *Mon. Wea. Rev.,* **125,** 1414–1430.

Holton, J. R., 1992: *An Introduction to Dynamic Meteorology.* 3d ed. Academic Press, 511 pp.

Huo, Z., D.-L. Zhang, J. Gyakum, and A. Staniforth, 1995: A diagnostic analysis of the Superstorm of March 1993. *Mon. Wea. Rev.,* **123,** 1740–1761.

Hurd, W. E., 1929: Northers of the Gulf of Tehuantepec. *Mon. Wea. Rev.,* **57,** 192–194.

Huschke, R. E., Ed., 1959: *Glossary of Meteorology.* Amer. Meteor. Soc., 638 pp.

Jackson, P. L., and D. G. Steyn, 1994a: Gap winds in a fjord. Part I: Observations and numerical simulation. *Mon. Wea. Rev.,* **122,** 2645–2665.

——, and ——, 1994b: Gap winds in a fjord. Part II: Hydraulic analog. *Mon. Wea. Rev.,* **122,** 2666–2676.

Jones, B., S. Boudjelas, and E. G. Mitchelson-Jacob, 1997: Topographic steering of winds in Vestfjorden, Norway. *Weather,* **52,** 304–311.

Kain, J. S., and J. M. Fritsch, 1993: Convective parameterization for mesoscale models: The Kain–Fritsch scheme. *The Representation of Cumulus Convection in Numerical Models, Meteor. Monogr.,* No. 46, Amer. Meteor. Soc., 165–170.

Klemp, J. B., and D. R. Durran, 1983: An upper boundary condition permitting internal gravity wave radiation in numerical mesoscale models. *Mon. Wea. Rev.,* **111,** 430–444.

Kocin, P. J., P. N. Schumacher, R. F. Morales Jr., and L. W. Uccellini, 1995: Overview of the 12–14 March 1993 Superstorm. *Bull. Amer. Meteor. Soc.,* **76,** 165–182.

Lackmann, G. M., and J. E. Overland, 1989: Atmospheric structure and momentum balance during a gap-wind event in Shelikof Strait, Alaska. *Mon. Wea. Rev.,* **117,** 1817–1833.

Legeckis, R., 1988: Upwelling off the Gulfs of Panama and Papagayo in the tropical Pacific during March 1985. *J. Geophys. Res.,* **93,** 15 485–15 489.

Lluch-Cota, S. E., S. Álvarez-Borrego, E. M. Santamaría-del Ángel, F. E. Müller-Karger, and S. Hernández-Vázquez, 1997: The Gulf of Tehuantepec and adjacent areas: Spatial and temporal variation of satellite-derived photosynthetic pigments. *Cienc. Mar.,* **23,** 329–340.

Mass, C. F., S. Businger, M. D. Albright, and Z. A. Tucker, 1995: A windstorm in the lee of a gap in a coastal mountain barrier. *Mon. Wea. Rev.,* **123,** 315–331.

McCreary, J. P., Jr., H. S. Lee, and D. B. Enfield, 1989: The response of the coastal ocean to strong offshore winds: With application to the Gulfs of Tehuantepec and Papagayo. *J. Mar. Res.,* **47,** 81–109.

Overland, J. E., 1984: Scale analysis of marine winds in straits and along mountainous coasts. *Mon. Wea. Rev.,* **112,** 2530–2534.

——, and B. A. Walter Jr., 1981: Gap winds in the Strait of Juan de Fuca. *Mon. Wea. Rev.,* **109,** 2221–2233.

Parmenter, F. C., 1970: A ''Tehuantepecer.'' *Mon. Wea. Rev.,* **98,** 479.

Powers, J. G., 1996: Coupling of the MM5 with marine models. Preprints, *Sixth PSU/NCAR Mesoscale Model Users' Workshop,* Boulder, CO, Mesoscale and Microscale Meteorology Division/National Center for Atmospheric Research, 53–57.

Reding, P. J., 1992: The Central American cold surge: An observational analysis of the deep south-ward penetration of North American cold fronts. M.S. thesis, Dept. of Meteorology, Texas A&M University, 177 pp. [Available from Dept. of Meteorology, Texas A&M University, College Station, TX 77843-3150.]

Reed, T. R., 1931: Gap winds of the Strait of Juan de Fuca. *Mon. Wea. Rev.,* **59,** 373–376.

Reid, S., 1996: Pressure gradients and winds in Cook Strait. *Wea. Forecasting,* **11,** 476–488.

Schoenberger, L. M., 1984: Doppler radar observation of a land–breeze cold front. *Mon. Wea. Rev.,* **112,** 2455–2464.

Schultz, D. M., W. E. Bracken, L. F. Bosart, G. J. Hakim, M. A. Bedrick, M. J. Dickinson, and K. R. Tyle, 1997: The 1993 Superstorm cold surge: Frontal structure, gap flow, and tropical impact. *Mon. Wea. Rev.,* **125,** 5–39; Corrigendum, **125,** 662.

——, ——, and ——, 1998: Planetary- and synoptic-scale signatures associated with Central American cold surges. *Mon. Wea. Rev.,* **126,** 5–27.

Scorer, R. S., 1952: Mountain-gap winds—A study of the surface wind at Gibraltar. *Quart. J. Roy. Meteor. Soc.,* **78,** 53–59.

Stauffer, D. R., and N. L. Seaman, 1990: Use of four-dimensional data assimilation in a limited-area mesoscale model. Part I: Experiments with synoptic-scale data. *Mon. Wea. Rev.,* **118,** 1250–1277.

Stumpf, H. G., 1975a: Satellite detection of upwelling in the Gulf of Tehuantepec, Mexico. *Mar. Wea. Log,* **19,** 71–74.

——, 1975b: Satellite detection of upwelling in the Gulf of Tehuantepec, Mexico. *J. Phys. Oceanogr.,* **5,** 383–388.

——, and R. V. Legeckis, 1977: Satellite observations of mesoscale eddy dynamics in the eastern tropical Pacific Ocean. *J. Phys. Oceanogr.,* **7,** 648–658.

Trasviña Castro, A.,1991: Offshore wind forcing in a coastal ocean: Observations and modeling of the Gulf of Tehuantepec, Mexico. Ph.D. thesis, University of Wales, 88 pp. [Available from School of Ocean Sciences, University of Wales Bangor, Menai Bridge, Gwynedd LL59 5EY, United Kingdom.]

——, E. D. Barton, J. Brown, H. S. Velez, P. M. Kosro, and R. L. Smith, 1995: Offshore wind forcing in the Gulf of Tehuantepec, Mexico: The asymmetric circulation. *J. Geophys. Res.,* **100,** 20 649–20 663.

Trenberth, K. E., 1992: Global analyses from ECMWF and atlas of 1000 to 10 mb circulation statistics. NCAR Tech. Note NCAR/TN-373+STR, 191 pp. [Available from UCAR Communications, P.O. Box 3000, Boulder, CO 80307.]

Uccellini, L. W., P. J. Kocin, R. S. Schneider, P. M. Stokols, and R. A. Door, 1995: Forecasting the 12–14 March 1993 Superstorm. *Bull. Amer. Meteor. Soc.,* **76,** 183–199.

Wolyn, P., 1994: The importance of cold, dry easterly Columbia Gorge winds for snowstorms in Portland, Oregon. Preprints, *Sixth Conf. on Mesoscale Processes,* Portland, OR, Amer. Meteor. Soc., 505–507.

Woodruff, S. D., R. J. Slutz, R. L. Jenne, and P. M. Steurer, 1987: A Comprehensive Ocean–Atmosphere Data Set. *Bull. Amer. Meteor. Soc.,* **68,** 1239–1250.

Zhang, D., and R. A. Anthes, 1982: A high-resolution model of the planetary boundary layer—Sensitivity tests and comparisons with SESAME-79 data. *J. Appl. Meteor.,* **21,** 1594–1609.